## PAPER

Check for updates

# Polymerization-induced self-assembly mediated by vinyl-functionalized macromolecular chain transfer agents: a straightforward approach to prepare cross-linked block copolymer nanoparticles with tunable morphologies†

Honggao Huang, [ID] ‡[a] Liwei Luo,‡[a] Li Zhang*[a,b] and Jianbo Tan [ID] *[a,b]

Herein, block-type and random-type vinyl-functionalized macromolecular reversible addition–fragmentation chain transfer (macro-RAFT) agents were synthesized by RAFT solution polymerization and employed to mediate aqueous photoinitiated RAFT dispersion polymerization of hydroxylpropyl methacrylate (HPMA). When using the block-type macro-RAFT agent, cross-linked block copolymer nanoparticles with various morphologies could be prepared. Control experiments demonstrate that the vinyl group in the macro-RAFT agent has little impact on the polymerization process and the morphology of block copolymer nanoparticles. The morphologies of block copolymer nanoparticles could be controlled by changing the length of the stabilizer block, the [HPMA]/[macro-RAFT] ratio, and the HPMA concentration. When using the random-type macro-RAFT agent, cross-linked block copolymer nanoparticles were still obtained. Moreover, it was found that the random distribution of vinyl groups in the macro-RAFT agent facilitated the formation of higher-order morphologies. Finally, the obtained cross-linked worms and vesicles were used as seeds for seeded RAFT polymerization of *tert*-butyl acrylate (*t*BA) or glycidyl methacrylate (GlyMA), which enables further control over the surface morphology of block copolymer nanoparticles. We expect that this study will offer new opportunities for the rational preparation of cross-linked block copolymer nanoparticles with various morphologies.

## Introduction

Over the past two decades or so, polymerization-induced self-assembly (PISA) *via* reversible addition–fragmentation chain transfer (RAFT) dispersion polymerization or RAFT emulsion polymerization has become a powerful technique for the rational preparation of block copolymer nanoparticles at high concentrations. This technique usually involves growing a solvophobic block from a solvophilic macromolecular RAFT (macro-RAFT) agent in a selective solvent. Once the solvophobic block reaches a critical molecular weight, nucleation occurs to generate block copolymer micelles, with the solvophilic block acting as a steric stabilizer. Unreacted monomers

diffuse into the micellar cores, leading to a relatively high monomer concentration inside the micelles and therefore the observed higher polymerization rate. The distinct nature of PISA enables high monomer conversions to be achieved within a relatively short time, which makes PISA an attractive method for scalable preparation of block copolymer nanoparticles.[1–27]

Typically, monofunctional macro-RAFT agents are employed to mediate RAFT-PISA to synthesize linear diblock copolymer nanoparticles.[28–39] The final morphology of block copolymer nanoparticles mainly depends on the volume ratio of the solvophilic and solvophobic blocks. Other reaction parameters such as solids content,[40,41] reaction temperature,[42–44] initiation type,[45] and solvent composition[46] also have significant influence on the morphology of block copolymer nanoparticles. Another useful strategy to control the morphology under RAFT-PISA conditions is the use of macro-RAFT agents with different structures.[21,24,26,47–55] For example, Cai *et al.*[52] compared the performance of an R-type branched macro-RAFT agent and a Z-type branched macro-RAFT during RAFT-PISA. For the R-type branched macro-RAFT agent, the solvophobic block always grows at the periphery of the formed branched block copolymers, leading to the occurrence of bridging

[a]Department of Polymeric Materials and Engineering, School of Materials and Energy, Guangdong University of Technology, Guangzhou 510006, China. E-mail: lizhang@gdut.edu.cn, tanjianbo@gdut.edu.cn
[b]Guangdong Provincial Key Laboratory of Functional Soft Condensed Matter, Guangzhou 510006, China

‡ These authors contributed equally to this work.

between particles and the observed precipitation. In contrast, for the Z-type branched macro-RAFT agent, the solvophobic block always grows at the inner structure of the formed branched block copolymers, and well-defined branched block copolymers and their assemblies were formed. It is apparent that the position of RAFT reactive groups in the macro-RAFT agent affects the self-assembled structures significantly. Besides the RAFT reactive group, the vinyl group is another reactive group that can participate in the RAFT polymerization. However, the use of a vinyl-functionalized macro-RAFT agent in RAFT-PISA has rarely been reported.

In this study, a series of vinyl-functionalized macro-RAFT agents with different numbers and distributions of vinyl groups were synthesized by RAFT polymerization. Block-type vinyl-functionalized macro-RAFT agents were synthesized by sequential RAFT solution polymerization of glycerol methacrylate (GMA) first and then allyl methacrylate (AMA). The random-type vinyl-functionalized macro-RAFT agent was synthesized directly by RAFT solution copolymerization of GMA and AMA. These vinyl-functionalized macro-RAFT agents were employed to mediate aqueous photoinitiated RAFT dispersion polymerization of HPMA to access a diverse set of cross-linked block copolymer nanoparticles with various morphologies. The effects of reaction parameters such as the monomer concentration, the [HPMA]/[macro-RAFT] ratio, and the distribution and number of vinyl groups on the RAFT-PISA process as well as the final morphology of block copolymer nanoparticles were studied in detail. Finally, seeded RAFT polymerization using the cross-linked worms and vesicles as seeds was also conducted to fabricate multicompartment polymer nanoparticles.

# Results and discussion

## Synthesis of vinyl-functionalized macro-RAFT agents

For the synthesis of block-type vinyl-functionalized macro-RAFT agents, RAFT solution polymerization of GMA mediated by 4-cyano-4-(ethylthiocarbonothioylthio)pentanoic acid (CEPA) was first performed to synthesize a large batch of $PGMA_n$-CEPA. $PGMA_n$-CEPA was then used to mediate RAFT solution polymerization of AMA (Scheme 1a). To ensure the retainment of the allylic units and eliminate the branching reaction,[56] the polymerization was quenched at a relatively low methacrylic unit conversion and the degree of polymerization (DP) of PAMA was determined by the conversion of the methacrylic unit via ^{1}H NMR spectroscopy. Fig. 1a shows $N,N$-dimethylformamide (DMF) size exclusion chromatography (SEC) traces of $PGMA_{45}$-CEPA, $PGMA_{45}$-$PAMA_{4.5}$-CEPA, and $PGMA_{45}$-$PAMA_{8.3}$-CEPA. The SEC trace shifted slightly to a lower elution volume (higher molecular weight) after the RAFT polymerization of AMA, indicating the successful chain extension of PAMA. Relatively narrow molecular weight distributions ($M_w/M_n \leq 1.36$) were observed in all cases, suggesting minimal occurrence of branching during the AMA polymerization. Fig. 1b shows ^{1}H NMR spectra of $PGMA_{45}$-CEPA, $PGMA_{45}$-$PAMA_{4.5}$-CEPA, and $PGMA_{45}$-$PAMA_{8.3}$-CEPA. The presence of proton signals at 5.90 ppm (peak b) and 5.20–5.50 ppm (peak a) confirms the retainment of the allylic units after RAFT polymerization. A random-type vinyl-functionalized macro-RAFT agent (P($GMA_{44}$-co-$AMA_5$)-CEPA) was also synthesized directly by RAFT solution polymerization of GMA and AMA. SEC analysis confirmed a number-average molecular weight ($M_n$) of 18.7 kg mol$^{-1}$ and a dispersity of 1.29.
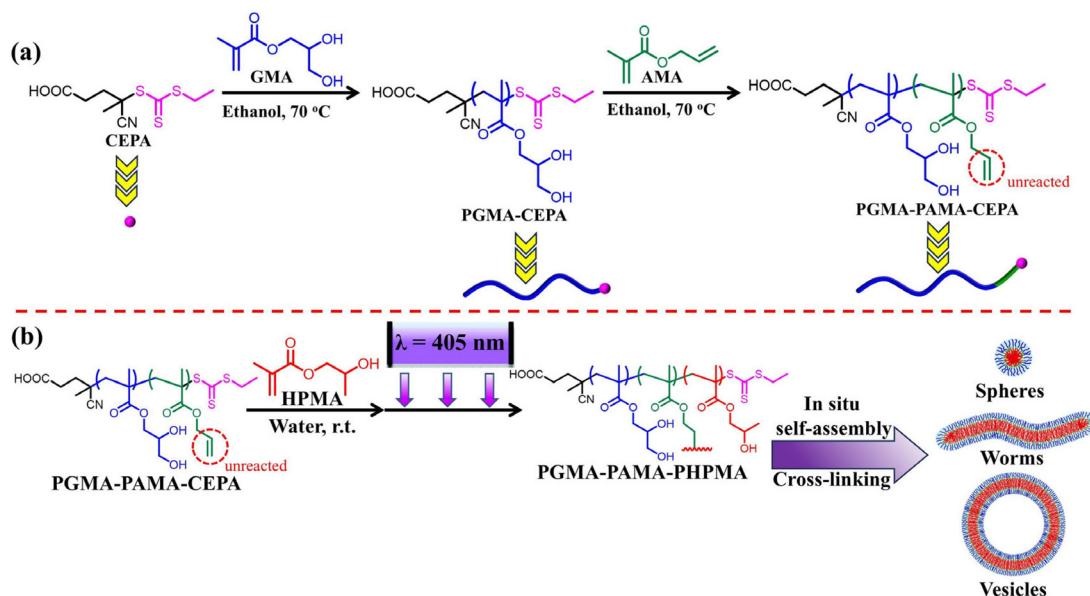


**Scheme 1** (a) Schematic illustration of the synthesis of block-type vinyl-functionalized macro-RAFT agents by RAFT solution polymerization. (b) Schematic illustration of the synthesis of cross-linked block copolymer nanoparticles by photoinitiated aqueous RAFT dispersion polymerization of HPMA using PGMA-PAMA-CEPA as the macro-RAFT agent.
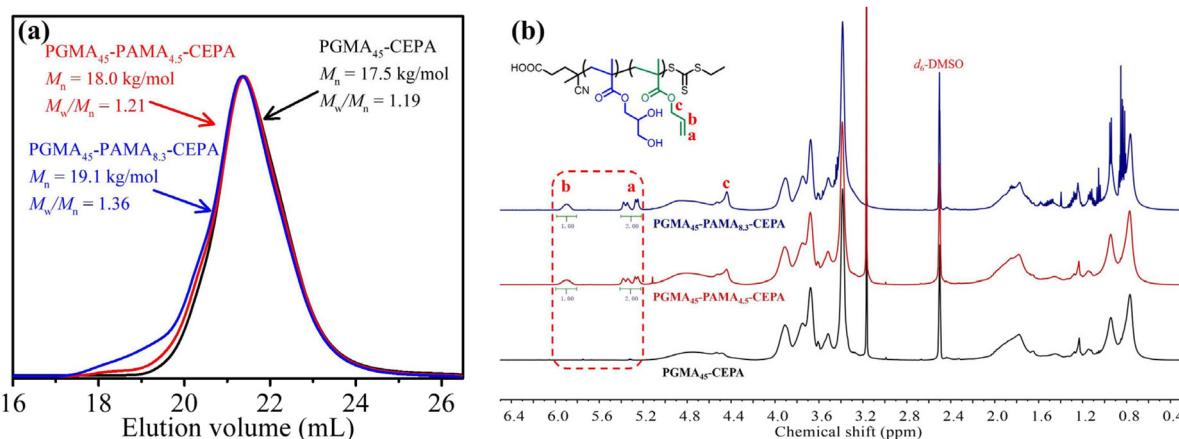
**Fig. 1** (a) DMF SEC traces and (b) $^1$H NMR spectra of PGMA$_{45}$-CEPA, PGMA$_{45}$-PAMA$_{4.5}$-CEPA, and PGMA$_{45}$-PAMA$_{8.3}$-CEPA.

The $^1$H NMR spectrum of P(GMA$_{44}$-co-AMA$_5$)-CEPA also verified the presence of the allylic unit in the macro-RAFT agent (Fig. S1†).

### Aqueous photoinitiated RAFT dispersion polymerization mediated by vinyl-functionalized macro-RAFT agents

For comparison, PGMA$_{45}$-CEPA was first used to mediate aqueous photoinitiated RAFT dispersion polymerization of HPMA (15% w/w) at room temperature with the [HPMA]/[PGMA$_{45}$-CEPA] ratio ranging from 100 to 250. Sodium phenyl-2,4,6-trimethylbenzoylphosphinate (SPTP) was used as the water-soluble photoinitiator under purple light irradiation ($\lambda$ = 405 nm, 0.45 mW cm$^{-2}$). In each case, high monomer conversion (>99%) was achieved within 30 min of purple light irradiation. The obtained polymers could be fully dissolved in DMF and were analyzed by DMF SEC. SEC analysis indicated that moderate RAFT control was achieved, with an increase in molecular weight and relatively broad molecular weight distributions being observed (Fig. 2e). The relatively high dispersities ($M_w/M_n$ = 1.33–1.73) can be attributed to the presence of a small amount of dimethacrylate impurity in the HPMA monomer that leads to light branching during the polymerization.[57] It should be noted that the tailing of SEC traces at 20–23 mL should be attributed to the presence of a certain amount of unreacted macro-CTA and this also increases the dispersities. At the [HPMA]/[PGMA$_{45}$-CEPA] ratio of 100, spherical micelles mixed with worms were formed (Fig. 2a). When the [HPMA]/[PGMA$_{45}$-CEPA] ratio was increased to 150 or 200, mixed morphologies of bilayers and vesicles were observed (Fig. 2b and c). Further increasing the [HPMA]/[PGMA$_{45}$-CEPA] ratio to 250 led to the formation of pure vesicles (Fig. 2d). These results are similar to those found in our previous research on aqueous photoinitiated RAFT dispersion polymerization of HPMA.[43,58]
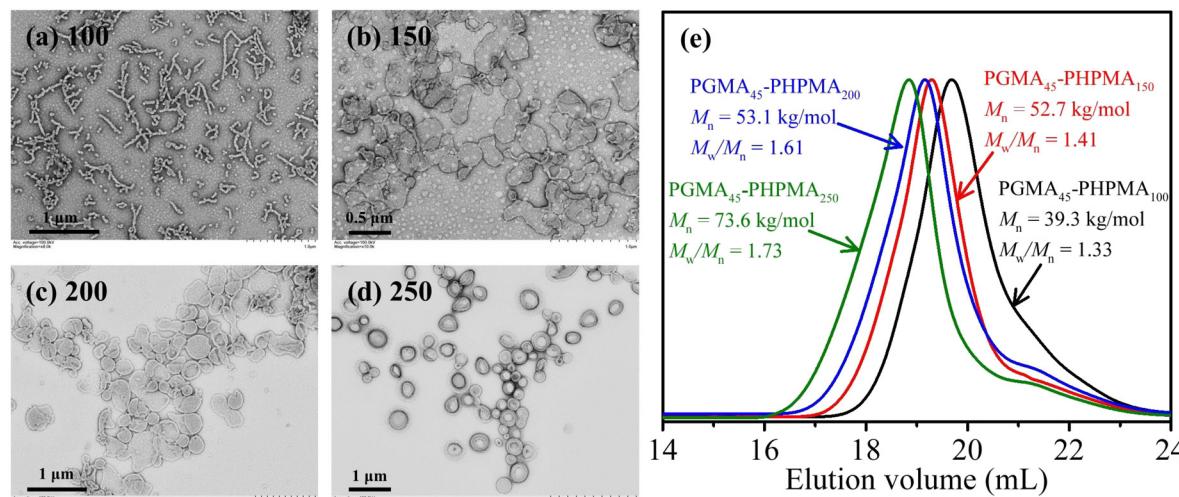


**Fig. 2** (a–d) TEM images of block copolymer nanoparticles prepared by photoinitiated RAFT dispersion polymerization of HPMA (15% w/w) in water using PGMA$_{45}$-CEPA with different [HPMA]/[PGMA$_{45}$-CEPA] ratios. (e) DMF SEC traces of block copolymers synthesized by photoinitiated RAFT dispersion polymerization of HPMA (15% w/w) in water using PGMA$_{45}$-CEPA with different [HPMA]/[PGMA$_{45}$-CEPA] ratios.

The vinyl-functionalized macro-RAFT agents, PGMA$_{45}$-PAMA$_{4.5}$-CEPA and PGMA$_{45}$-PAMA$_{8.3}$-CEPA, were then employed to mediate aqueous photoinitiated RAFT dispersion polymerization of HPMA (15% w/w) at room temperature with different [HPMA]/[macro-RAFT] ratios. $^1$H NMR analysis confirmed that near quantitative monomer conversion was achieved in each case after 30 min of light irradiation. In all cases, colloidally stable dispersions were obtained. Fig. 3 shows TEM images of the formed block copolymer nanoparticles. Mixed morphologies of spheres and short worms were observed at the [HPMA]/[macro-RAFT] ratio of 100 (Fig. 3a and e). At the [HPMA]/[macro-RAFT] ratio of 150, mixed morphologies of spheres, short worms, and bilayers were observed (Fig. 3b and f). When the [HPMA]/[macro-RAFT] ratio was increased to 200, vesicles mixed with bilayers were formed (Fig. 3c and g). Further increasing the [HPMA]/[macro-RAFT] ratio to 250 led to the formation of pure vesicles (Fig. 3d and h). These results suggest that the DP of the PAMA block should have little influence on the morphology of block copolymer nanoparticles. However, we found that the block copolymer nanoparticles prepared by using PGMA$_{45}$-PAMA$_n$-CEPA cannot dissolve in DMF (a good solvent for both PGMA-PAMA and PHPMA) for SEC analysis. We hypothesized that the allylic units of the macro-RAFT agent could participate in the RAFT dispersion polymerization of HPMA to form a cross-linked network within the block copolymer nanoparticles and this will be demonstrated in the following section. It should be noted that the *in situ* preparation of cross-linked block copolymer nanoparticles by RAFT-PISA has been reported by other groups.[17,33,59–62] For example, the An group[33,60] reported the synthesis of cross-linked worms and vesicles by RAFT dispersion polymerization by adding an asymmetrical cross-linker such as AMA in the polymerization system. Chen *et al.*[61] also synthesized pH- and reduction-responsive vesicles by RAFT-PISA by adding a symmetrical cross-linker with lower reactivity. However, the direct preparation of cross-linked block copolymer nanoparticles by RAFT-PISA using a vinyl-functionalized macro-RAFT agent has not yet been reported before.

With this established approach, one can directly prepare cross-linked block copolymer nanoparticles with various morphologies. For a typical PISA formulation, some important parameters such as the length of the stabilizer block have proved to affect the morphology of block copolymer nanoparticles significantly.[40,63] Herein, we also investigated the effect of the stabilizer block on the morphology of cross-linked block copolymer nanoparticles. PGMA$_{30}$-PAMA$_{8.9}$-CEPA (Fig. S2†) and PGMA$_{56}$-PAMA$_{9.5}$-CEPA (Fig. S3†) were also synthesized and employed to mediate aqueous photoinitiated RAFT dispersion polymerization of HPMA (15% w/w) with the [HPMA]/[macro-RAFT] ratio ranging from 100 to 250. Fig. 4a–d show block copolymer nanoparticles prepared by using PGMA$_{30}$-PAMA$_{8.9}$-CEPA with different [HPMA]/[macro-RAFT] ratios. At the [HPMA]/[macro-RAFT] ratio of 100, worms mixed with bilayers were formed (Fig. 4a). At the [HPMA]/[macro-RAFT] ratio of 150, bilayers were observed (Fig. 4b). Pure vesicles could be obtained when the [HPMA]/[macro-RAFT] ratio reached 200 or higher (Fig. 4c and d). By using PGMA$_{56}$-PAMA$_{9.5}$-CEPA as the macro-RAFT agent, pure spheres were formed at the [HPMA]/[macro-RAFT] ratio of 200 or lower (Fig. 4e–g). Further increasing the [HPMA]/[macro-RAFT] ratio to 250 led to the formation of a mixed morphology of spheres and necklace-like (or worm-like) particles (Fig. 4h). The necklace-like particles should be formed from the incomplete fusion of spherical micelles. The results in Fig. 3 demonstrated that the minor difference in the degree of polymerization (DP) of the PAMA block should have little influence on the morphology of block copolymer nanoparticles. Comparing Fig. 3e–h and 4, it can be concluded that using a longer stabilizer block should facilitate the formation of lower-order morphologies. This is because the longer stabilizer block can provide more efficient steric stabilization toward micelles, which can inhibit the fusion between micelles and therefore
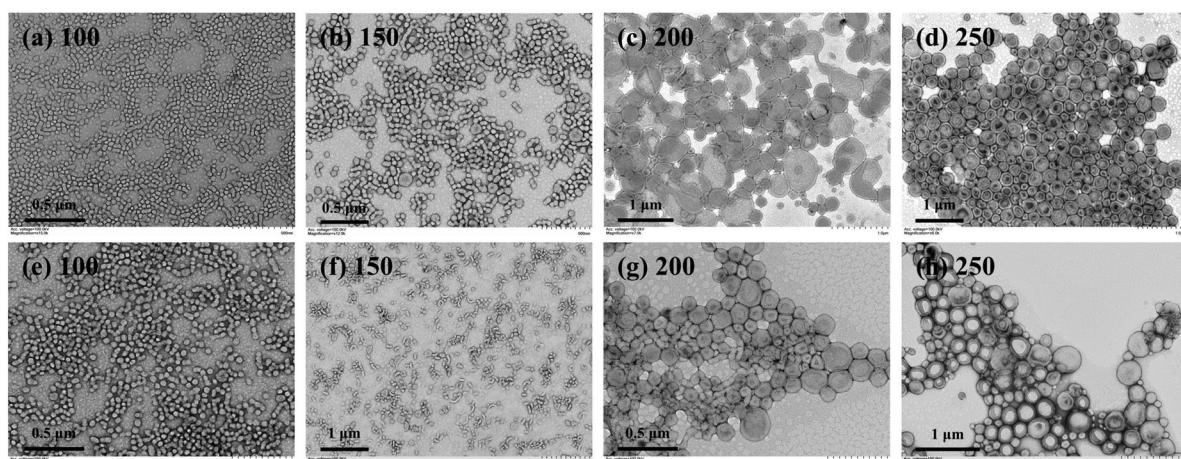


**Fig. 3** (a–d) TEM images of block copolymer nanoparticles prepared by photoinitiated RAFT dispersion polymerization of HPMA (15% w/w) in water using PGMA$_{45}$-PAMA$_{4.5}$-CEPA with different [HPMA]/[macro-RAFT] ratios. (e–h) TEM images of block copolymer nanoparticles prepared by photoinitiated RAFT dispersion polymerization of HPMA (15% w/w) in water using PGMA$_{45}$-PAMA$_{8.3}$-CEPA with different [HPMA]/[macro-RAFT] ratios.
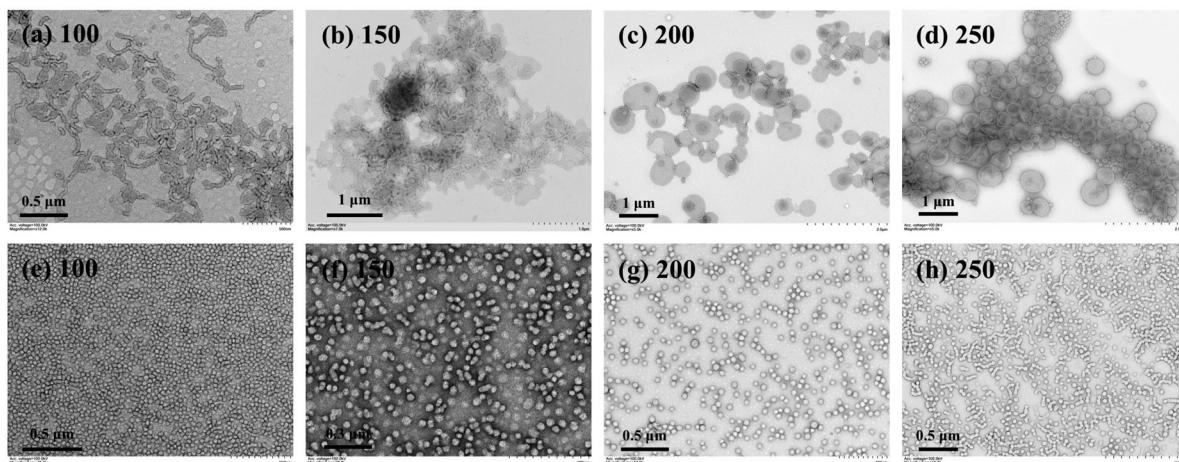
**Fig. 4** (a–d) TEM images of block copolymer nanoparticles prepared by photoinitiated RAFT dispersion polymerization of HPMA (15% w/w) in water using $PGMA_{30}$-$PAMA_{8.9}$-CEPA with different [HPMA]/[macro-RAFT] ratios. (e–h) TEM images of block copolymer nanoparticles prepared by photoinitiated RAFT dispersion polymerization of HPMA (15% w/w) in water using $PGMA_{56}$-$PAMA_{9.5}$-CEPA with different [HPMA]/[macro-RAFT] ratios.

the formation of lower-order morphologies. Besides the length of the stabilizer block, monomer concentration is another important parameter that affects the morphology of block copolymer nanoparticles prepared by PISA.[43] In this study, a morphological phase diagram was also constructed for block copolymer nanoparticles prepared by aqueous photoinitiated RAFT dispersion polymerization of HPMA mediated by $PGMA_{45}$-$PAMA_{8.3}$-CEPA *via* the systematic variation of the [HPMA]/[macro-RAFT] ratio and the HPMA concentration. As shown in Fig. 5, this morphological phase diagram is concentration-dependent, which is similar to traditional PISA formulations.[40,43] Only mixed morphologies of spheres and worm-like particles could be accessed at the HPMA concentration of 10% w/w. This can be attributed to the reduced possibility of fusion between particles that inhibits the formation of higher-order morphologies. Pure vesicles were typically observed at the [HPMA]/[macro-RAFT] ratio of 200 or higher with the HPMA concentration of 15% w/w or higher. It

should be noted that cross-linked block copolymer nanoparticles could be obtained in all cases regardless of the [HPMA]/[macro-RAFT] ratio and the HPMA concentration. In other previously reported PISA formulations with AMA being added as an asymmetrical cross-linker,[64–66] it was found that the presence of AMA had no influence on the morphology of block copolymer nanoparticles. This can be attributed to the low reactivity of the allyl group of AMA that can delay the occurrence of cross-linking during the polymerization. Therefore, it is expected that the allyl groups in the $PGMA_{45}$-$PAMA_{8.3}$-CEPA macro-RAFT agent should also mainly be involved in the late stage of polymerization.

To further understand the effect of allylic units on the polymerization process, the polymerization kinetics of aqueous photoinitiated RAFT dispersion polymerization of HPMA (15% w/w) mediated by $PGMA_{45}$-CEPA or $PGMA_{45}$-$PAMA_{8.3}$-CEPA ([HPMA]/[macro-RAFT] = 250) were then analyzed. Aliquots were extracted at pre-determined time intervals
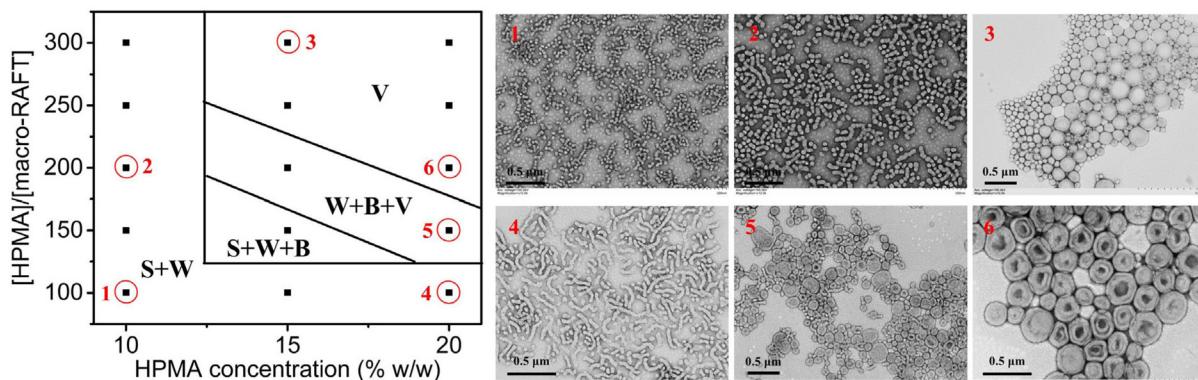


**Fig. 5** Morphological phase diagram of block copolymer nanoparticles prepared by photoinitiated RAFT dispersion polymerization of HPMA mediated by $PGMA_{45}$-$PAMA_{8.3}$-CEPA by varying the HPMA concentration and the [HPMA]/[macro-RAFT] ratio. Phase regions consist of spheres (S), worms (W), bilayers (B), and vesicles (V).

under a nitrogen atmosphere and diluted with $D_2O$ for $^1H$ NMR analysis. High rates of polymerization were observed in both cases with near quantitative monomer conversion being achieved within 15 min of light irradiation (Fig. 6a). This can be attributed to the fast decomposition of SPTP under purple light irradiation.[67] It was found that the presence of allylic units has little influence on the polymerization kinetics. Two distinct regimes were observed in the corresponding $\ln([M]_0/[M])$ vs. irradiation time plots (Fig. 6b), which is commonly observed in other PISA formulations.[57] After the micellar nucleation stage, the polymerization using PGMA$_{45}$-PAMA$_{8.3}$-CEPA was slower than that using PGMA$_{45}$-CEPA. We hypothesized that the reaction of allylic units would lead to the generation of cross-linked micelles that inhibits the diffusion of monomers into the micellar cores and therefore the decrease in polymerization rate. Moreover, the well-known stability of the allylic radicals could also play a role in the slower kinetics of polymerization.[68] Although cross-linked block copolymer nanoparticles formed at the end of polymerization when using

PGMA$_{45}$-PAMA$_{8.3}$-CEPA, soluble copolymers generated during the polymerization could still be analyzed by SEC. In this case, the polymers obtained at 9 min or before could be dissolved in DMF for SEC analysis. As shown in Fig. 6c, $M_n$ increased linearly with monomer conversion, although relatively broad molecular weight distributions were observed throughout the polymerization. Fig. 6d shows SEC traces of these samples, and an obvious high-molecular-weight shoulder was observed in the SEC trace obtained at 2 min, suggesting that branching has occurred at this time point. The SEC results indicate that the pendent allylic units in the macro-RAFT agent were partially involved in the RAFT dispersion polymerization of HPMA during the early stage, which can be attributed to the relatively low reactivity of the allylic units.[69] This is important since a denser cross-linked network formed in the early stage would limit the chain re-organization and the subsequent morphological transition.[59,60,64] The tailing of SEC traces at 20–23 mL should also be attributed to the presence of a certain amount of unreacted macro-CTA. The withdrawn samples were also
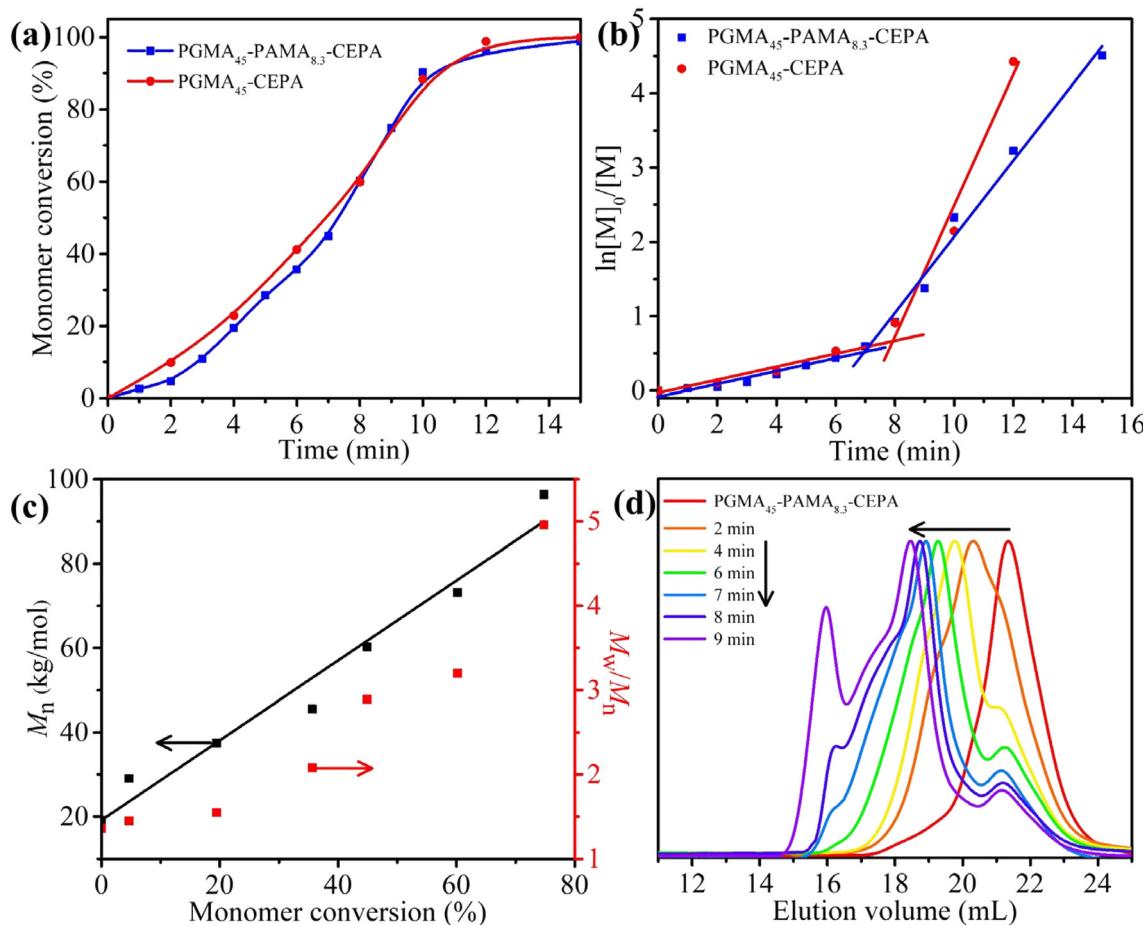


**Fig. 6** (a) Polymerization kinetics for aqueous photoinitiated RAFT dispersion polymerization of HPMA (15% w/w) mediated by PGMA$_{45}$-CEPA or PGMA$_{45}$-PAMA$_{8.3}$-CEPA with the [HPMA]/[macro-RAFT] ratio of 250. (b) Plots of $\ln([M]_0/[M])$ vs. irradiation time for aqueous photoinitiated RAFT dispersion polymerization of HPMA (15% w/w) mediated by PGMA$_{45}$-CEPA or PGMA$_{45}$-PAMA$_{8.3}$-CEPA with the [HPMA]/[macro-RAFT] ratio of 250. (c) Evolution of $M_n$ and $M_w/M_n$ with monomer conversion for samples obtained during the aqueous photoinitiated RAFT dispersion polymerization of HPMA (15% w/w) using PGMA$_{45}$-PAMA$_{8.3}$-CEPA. (d) DMF SEC traces of polymers obtained at different times during the aqueous photoinitiated RAFT dispersion polymerization of HPMA (15% w/w) using PGMA$_{45}$-PAMA$_{8.3}$-CEPA.
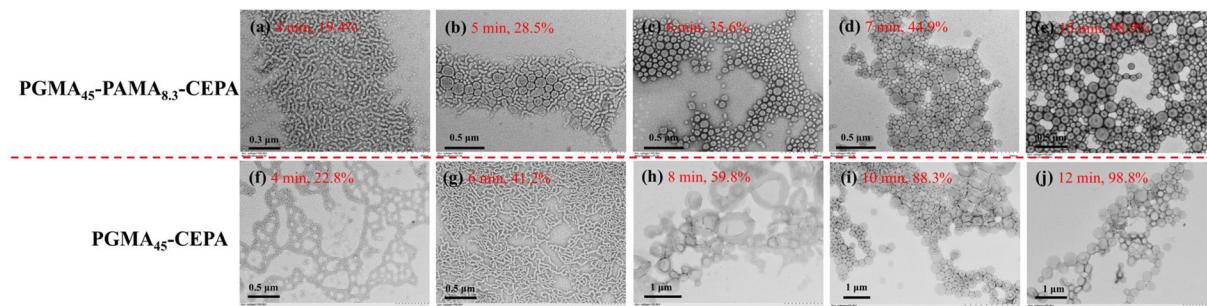
**Fig. 7** (a–e) TEM images of polymer nanoparticles obtained during the kinetic study of aqueous photoinitiated RAFT dispersion polymerization of HPMA (15% w/w) mediated by PGMA$_{45}$-PAMA$_{8.3}$-CEPA with the [HPMA]/[macro-RAFT] ratio of 250. (f–j) TEM images of polymer nanoparticles obtained during the kinetic study of aqueous photoinitiated RAFT dispersion polymerization of HPMA (15% w/w) mediated by PGMA$_{45}$-CEPA with the [HPMA]/[macro-RAFT] ratio of 250.

diluted with water and characterized by TEM, as shown in Fig. 7. In the case of using PGMA$_{45}$-PAMA$_{8.3}$-CEPA (Fig. 7a–e), the morphology transformed from spheres and short worms at 4 min (monomer conversion = 19.4%) to a mixed morphology of spheres, worms, and bilayers at 5 min (monomer conversion = 28.5%). At 6 min (monomer conversion = 35.6%), spheres mixed with vesicles were observed. As the polymerization proceeded further, pure vesicles were formed after 7 min (monomer conversion = 44.9%). A similar morphological transition process was observed for the polymerization using PGMA$_{45}$-CEPA (Fig. 7f–j), suggesting that the pendent allylic units in the macro-RAFT agent have little influence on morphological transition during the PISA process.

Since the allylic units can participate during RAFT dispersion polymerization of HPMA, it is expected that the distribution of allylic units in the macro-RAFT agent should also have significant effects on the PISA process as well the morphology of polymer nanoparticles. The random-type macro-RAFT agent, P(GMA$_{44}$-co-AMA$_5$)-CEPA, was then used to mediate aqueous photoinitiated RAFT dispersion polymerization of HPMA (10% w/w) with the [HPMA]/[macro-RAFT] ratio ranging from 150 to 300. At the [HPMA]/[macro-RAFT] ratio of 150, aggregates of vesicles with large sizes were observed (Fig. 8b). When the [HPMA]/[macro-RAFT] ratio was increased to 200 or higher, it led to the formation of pure vesicles (Fig. 8c–e). For comparison, PGMA$_{45}$-PAMA$_{4.5}$-CEPA and PGMA$_{45}$-PAMA$_{8.3}$-CEPA were also employed to mediate aqueous photoinitiated RAFT dispersion polymerization of HPMA (10% w/w). As shown in Fig. S4,† spheres mixed with necklace-like particles were formed at all investigated [HPMA]/[macro-RAFT] ratios. These results suggest that the random distribution of vinyl groups in the macro-RAFT agent could facilitate the formation of higher-order morphologies. This can be explained by the fact that the random grafted PHPMA chains in the macro-RAFT agent could promote the bridging between particles (Fig. 8a),[24,70] which has proved to be a critical step for the formation of higher-order morphologies.[57] This effect can be suppressed when using the block-type vinyl-functionalized macro-RAFT agent. Under aqueous RAFT dispersion polymerization conditions, the main polymerization

locus should be inside the monomer-swollen micelles after the nucleation stage.[57] Therefore, the pendent allylic units in the block-type vinyl-functionalized macro-RAFT agent should be consumed faster than those in the random-type vinyl-functionalized macro-RAFT agent. However, we failed to determine the conversion of the allylic units by ^{1}H NMR spectroscopy due to the low content of allylic units in the polymerization system. Nevertheless, the distribution of vinyl groups in the macro-RAFT agent can be an effective parameter to tune morphologies of cross-linked polymer nanoparticles prepared by RAFT-PISA. P(GMA$_{44}$-co-AMA$_5$)-CEPA can also be employed to synthesize inverse morphologies by increasing the HPMA concentration to 20% w/w (Fig. 8f–i), which is challenging for aqueous photoinitiated RAFT dispersion polymerization using other macro-RAFT agents.

The polymerization kinetics of aqueous photoinitiated RAFT dispersion polymerization of HPMA (10% w/w, [HPMA]/ [macro-RAFT] = 250) using P(GMA$_{44}$-co-AMA$_5$)-CEPA were also analyzed. Similar to the case of using PGMA$_{45}$-PAMA$_{8.3}$-CEPA, a high polymerization rate was also observed with quantitative monomer conversion being achieved within 15 min of light irradiation (Fig. 9a). Despite less allylic units in P(GMA$_{44}$-co-AMA$_5$)-CEPA than in PGMA$_{45}$-PAMA$_{8.3}$-CEPA, the cross-linking reaction occurred faster in the case of P(GMA$_{44}$-co-AMA$_5$)-CEPA and cross-linked polymers were obtained at a HPMA conversion of 51.0% or higher. This can be explained by the fact that the random distribution of allylic units in the macro-RAFT agent should be beneficial for the formation of a cross-linked polymer network. Soluble copolymers obtained at low HPMA conversions were then analyzed by DMF SEC (Fig. 9b and c). Upon increasing the polymerization time, the SEC trace shifted to a lower elution volume (higher molecular weight), suggesting the successful chain extension of PHPMA. Multimodal SEC traces were observed in all cases, which can be attributed to the grafting of PHPMA chains to the macro-RAFT agent. Samples obtained at different times were also analyzed by TEM. As shown in Fig. 9d–g, spheres were observed at 6 min or before (monomer conversion of 38.7% or lower) and sharply evolved to vesicles at 7 min (monomer conversion of 51.0%). Different from the cases of PGMA$_{45}$-CEPA and
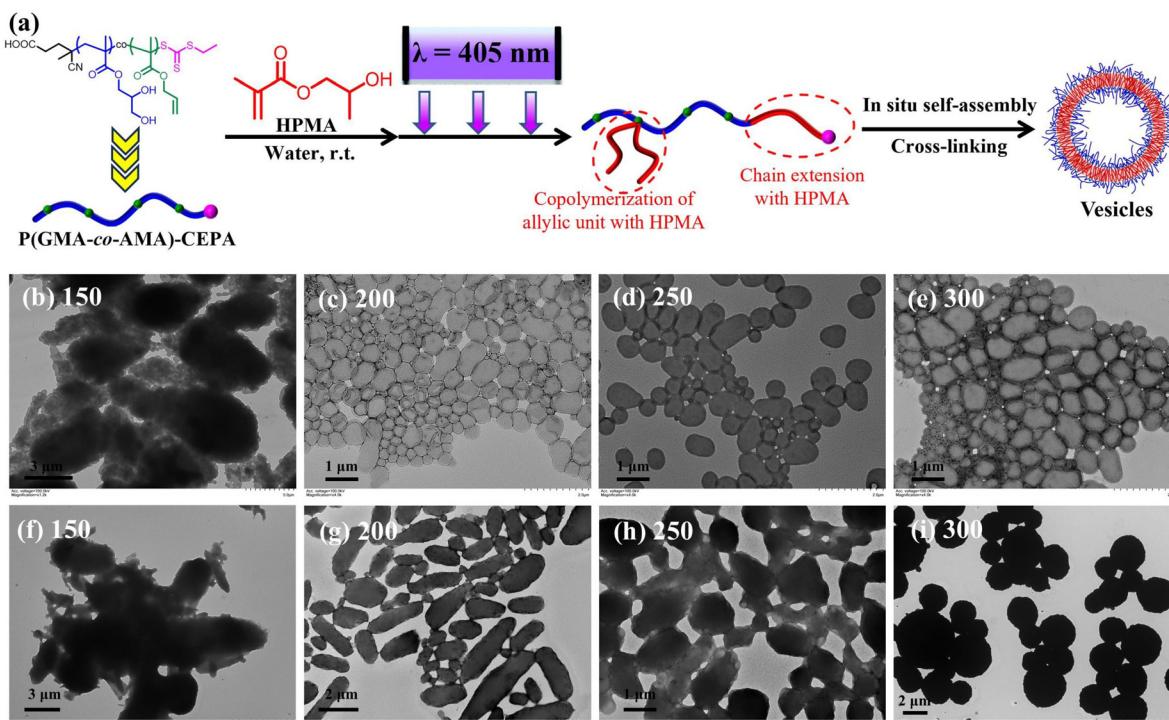
**Fig. 8** (a) Schematic illustration of aqueous photoinitiated RAFT dispersion polymerization of HPMA using P(GMA-*co*-AMA)-CEPA as the macro-RAFT agent. (b–e) TEM images of polymer nanoparticles prepared by aqueous photoinitiated RAFT dispersion polymerization of HPMA (10% w/w) using P(GMA$_{44}$-*co*-AMA$_5$)-CEPA with different [HPMA]/[macro-RAFT] ratios. (f–i) TEM images of polymer nanoparticles prepared by aqueous photoinitiated RAFT dispersion polymerization of HPMA (20% w/w) using P(GMA$_{44}$-*co*-AMA$_5$)-CEPA with different [HPMA]/[macro-RAFT] ratios.
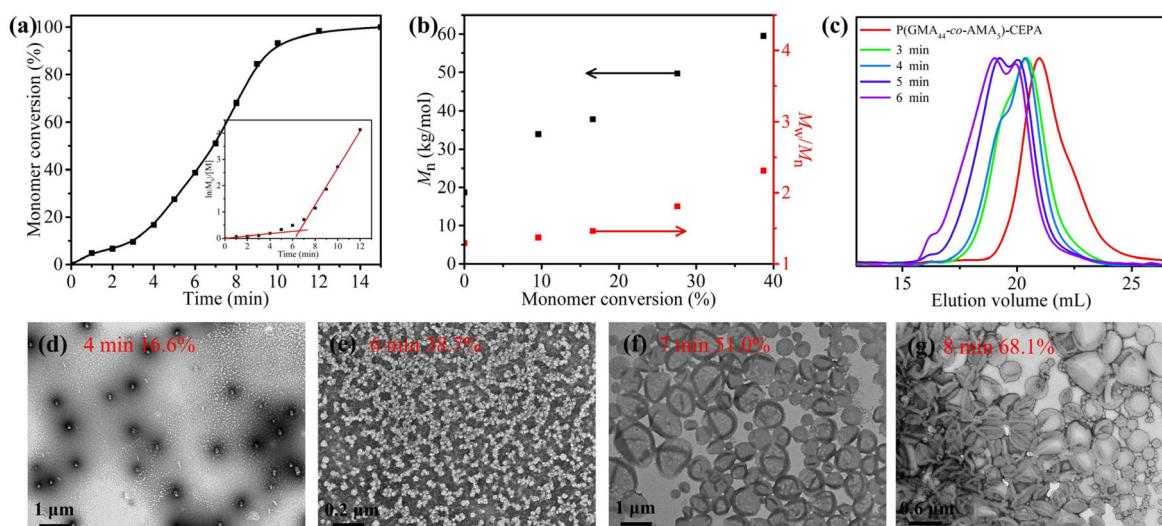


**Fig. 9** (a) Polymerization kinetics for aqueous photoinitiated RAFT dispersion polymerization of HPMA (10% w/w) mediated by P(GMA$_{44}$-*co*-AMA$_5$)-CEPA with the [HPMA]/[macro-RAFT] ratio of 250. (b) Evolution of $M_n$ and $M_w/M_n$ with monomer conversion for samples obtained during the aqueous photoinitiated RAFT dispersion polymerization of HPMA (10% w/w) using P(GMA$_{44}$-*co*-AMA$_5$)-CEPA. (c) DMF SEC traces of polymers obtained at different times during the aqueous photoinitiated RAFT dispersion polymerization of HPMA (10% w/w) using P(GMA$_{44}$-*co*-AMA$_5$)-CEPA. (d–g) TEM images of polymer nanoparticles obtained during the kinetic study of aqueous photoinitiated RAFT dispersion polymerization of HPMA (10% w/w) using P(GMA$_{44}$-*co*-AMA$_5$)-CEPA.

PGMA$_{45}$-PAMA$_{8.3}$-CEPA, no worm phase was observed at all investigated irradiation times. It is well known that the fusion between particles is critical for the morphological evolution to higher-order morphologies under PISA conditions.[57] During the early stage of polymerization (prior to cross-linking), the random distribution of allylic units in the macro-RAFT agent
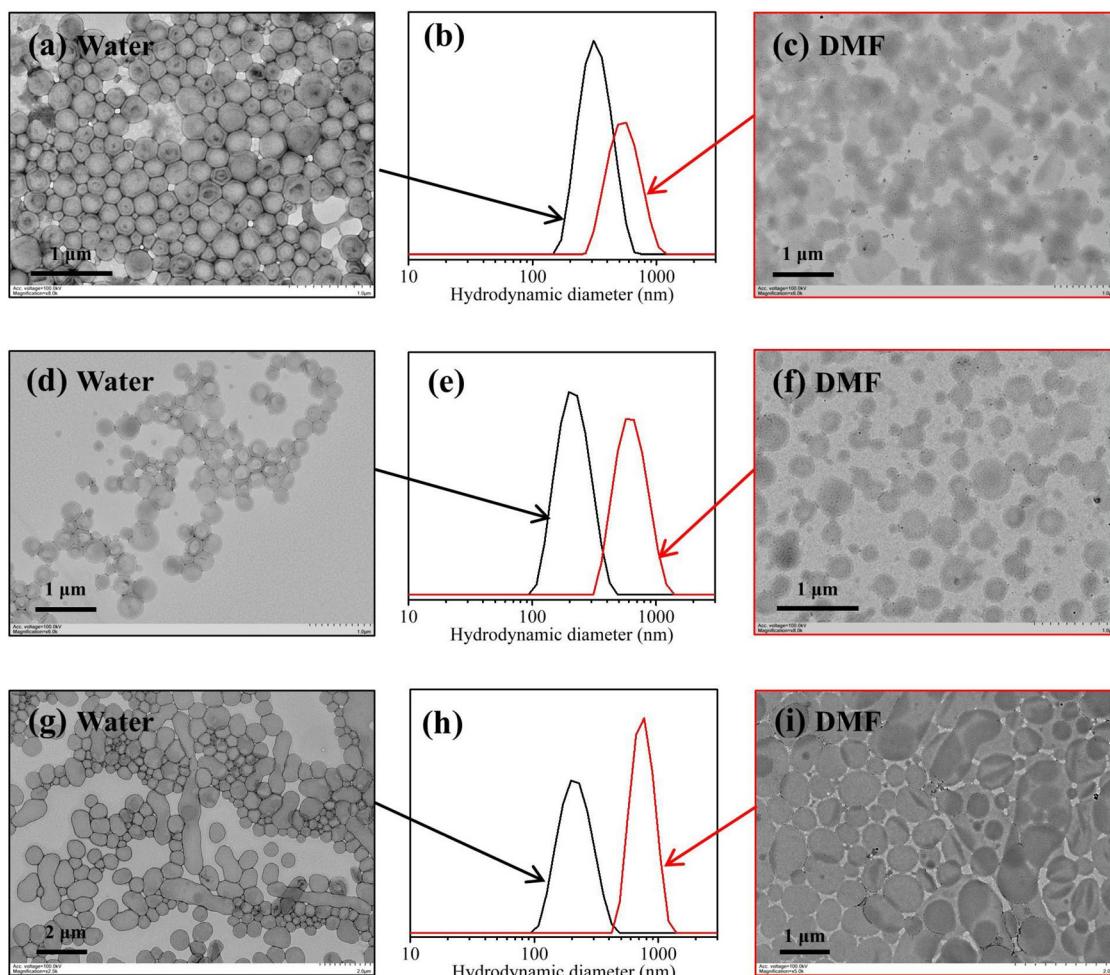
**Fig. 10** (a and c) TEM images and (b) DLS distributions of PGMA$_{45}$-PAMA$_{4.5}$-PHPMA$_{200}$ vesicles before and after dispersing in DMF. (d and f) TEM images and (e) DLS distributions of PGMA$_{45}$-PAMA$_{8.3}$-PHPMA$_{200}$ vesicles before and after dispersing in DMF. (g and i) TEM images and (h) DLS distributions of P(GMA$_{44}$-$co$-AMA$_5$)-PHPMA$_{200}$ vesicles before and after dispersing in DMF.

would lead to the generation of grafted copolymers with randomly distributed PHPMA side chains. According to our previous studies on RAFT-PISA of non-linear polymers,[53,70] such structures should be beneficial for the fusion between particles and therefore promote the formation of higher-order morphologies.

Fig. 10 shows TEM images of PGMA$_{45}$-PAMA$_{4.5}$-PHPMA$_{200}$ vesicles (prepared at 20% w/w HPMA) (Fig. 10a and c), PGMA$_{45}$-PAMA$_{8.3}$-PHPMA$_{200}$ vesicles (prepared at 20% w/w HPMA) (Fig. 10d and f), and P(GMA$_{44}$-$co$-AMA$_5$)-PHPMA$_{200}$ vesicles (prepared at 10% w/w HPMA) (Fig. 10g and i) before and after dispersing in DMF. It was found that the original vesicular morphologies were unchanged for these samples after dispersing in DMF, indicating that these vesicles were cross-linked after the polymerization. Dispersing these vesicles in DMF all resulted in a significant increase in the intensity-average diameter due to the swelling of vesicles in DMF (Fig. 10b, e and h). These results suggest that cross-linking occurred during aqueous photoinitiated RAFT dispersion polymerization mediated by vinyl-functionalized macro-RAFT

agents and therefore promotes the formation of cross-linked block copolymer nanoparticles. The formed vesicles also exhibited excellent long-range stability. For example, the P(GMA$_{44}$-$co$-AMA$_5$)-PHPMA$_{200}$ vesicles could maintain the vesicular morphology in water and DMF even after storage at room temperature for 6 months (Fig. S5†).

### Seeded RAFT polymerization using the cross-linked block copolymer nanoparticles as seeds

The above results demonstrate that one could easily prepare a diverse set of cross-linked block copolymer nanoparticles by RAFT dispersion polymerization using vinyl-functionalized macro-RAFT agents. Since a certain number of RAFT groups are embedded inside the core-forming block, the cross-linked block copolymer nanoparticles can be used as seeds for seeded RAFT polymerization to fabricate multicompartment block copolymer nanoparticles with unique morphologies.

Firstly, PGMA$_{45}$-PAMA$_{4.5}$-PHPMA$_{125}$ worms (Fig. 11a) prepared at a HPMA concentration of 20% w/w were used as seeds for aqueous photoinitiated seeded RAFT polymerization of
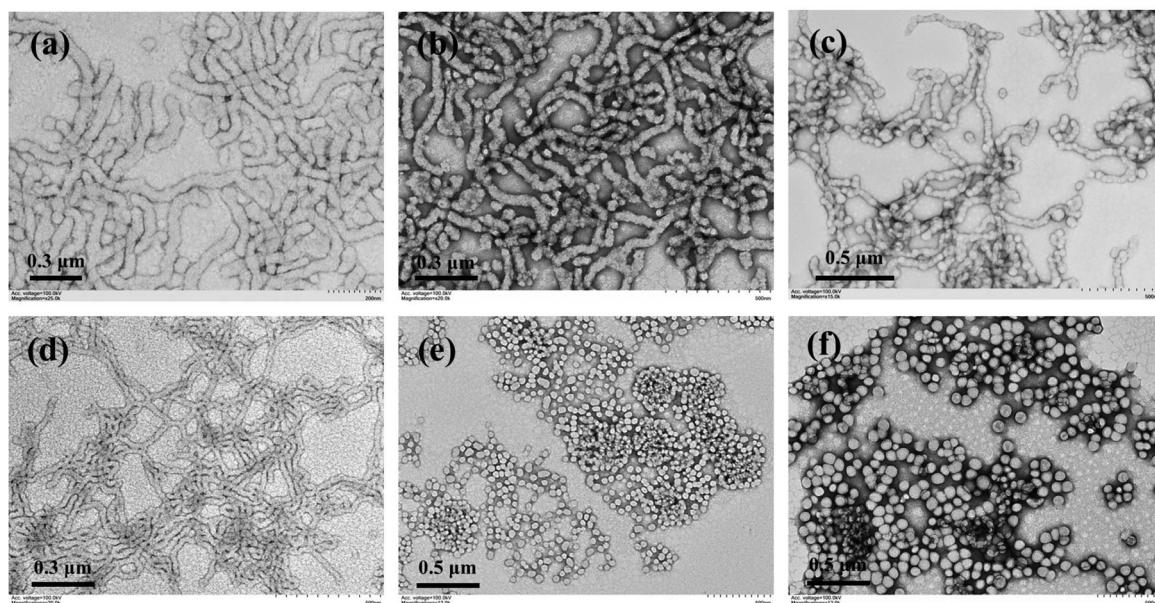
**Fig. 11** (a) TEM image of PGMA$_{45}$-PAMA$_{4.5}$-PHPMA$_{125}$ worms prepared by aqueous photoinitiated RAFT dispersion polymerization of HPMA (20% w/w). (b and c) TEM images of polymer nanoparticles prepared by photoinitiated seeded RAFT polymerization of $t$BA in water using PGMA$_{45}$-PAMA$_{4.5}$-PHPMA$_{125}$ worms as seeds with the [$t$BA]/[PGMA$_{45}$-PAMA$_{4.5}$-PHPMA$_{125}$] ratio of (b) 100 or (c) 300. (d) TEM image of PGMA$_{45}$-PHPMA$_{100}$ worms prepared by aqueous photoinitiated RAFT dispersion polymerization of HPMA (20% w/w). (e and f) TEM images of polymer nanoparticles prepared by photoinitiated seeded RAFT polymerization of $t$BA in water using PGMA$_{45}$-PHPMA$_{100}$ worms as seeds with the [$t$BA]/[PGMA$_{45}$-PHPMA$_{100}$] ratio of (e) 100 or (f) 300.

*tert*-butyl acrylate ($t$BA). Due to the hydrophobic nature of $t$BA, the polymerization should proceed under seeded RAFT emulsion polymerization conditions.[71] $^1$H NMR analysis confirmed that high monomer conversions were achieved within 1 h of light irradiation. When the DP of P$t$BA was 100, the worm-like morphology was maintained while the surface of worms became rough (Fig. 11b). On increasing the P$t$BA DP to 300,

the surface roughness of worms also increased (Fig. 11c). This can be explained by the fact that nanoscale phase separation occurred inside worms during seeded RAFT polymerization of $t$BA due to the incompatibility between PHPMA and P$t$BA.[65,72] Since the worm phase only occupies a very narrow region in the PISA-based morphological phase diagram,[40] a minor variation of the core-forming block would lead to the change of
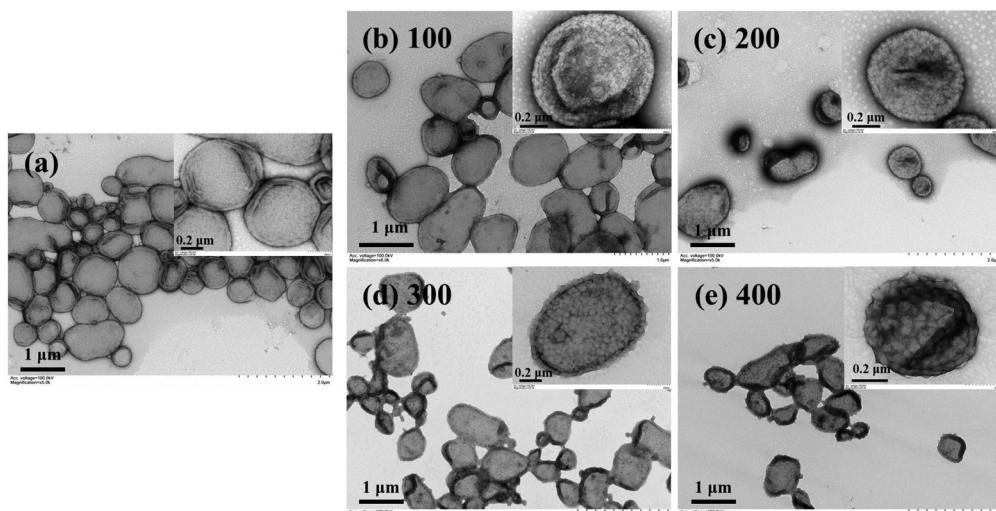


**Fig. 12** (a) TEM image of P(GMA$_{44}$-$co$-AMA$_5$)-PHPMA$_{250}$ vesicles prepared by aqueous photoinitiated RAFT dispersion polymerization of HPMA (10% w/w). (b–e) TEM images of framboidal vesicles prepared by photoinitiated seeded RAFT polymerization of GlyMA in water using P(GMA$_{44}$-$co$-AMA$_5$)-PHPMA$_{250}$ vesicles as seeds with different [GlyMA]/[P(GMA$_{44}$-$co$-AMA$_5$)-PHPMA$_{250}$] ratios.

morphology. Therefore, we believe that the cross-linked network of worms should play an important role in maintaining the worm-like morphology after seeded RAFT polymerization of *t*BA. As a control experiment, non-cross-linked PGMA$_{45}$-PHPMA$_{100}$ worms (Fig. 11d) were also used as seeds for seeded RAFT polymerization of *t*BA. In this case, worms fragmented into spherical micelles after seeded RAFT polymerization due to the increased surface tension after the chain extension of P*t*BA (Fig. 11e and f).[73] Besides worms, P(GMA$_{44}$-*co*-AMA$_5$)-PHPMA$_{250}$ vesicles (Fig. 12a) prepared at the HPMA concentration of 10% w/w were also used as seeds for seeded RAFT polymerization of glycidyl methacrylate (GlyMA) with different PGlyMA DPs. It was found that phase separation occurred within the vesicular membrane and framboidal vesicles were formed at all investigated PGlyMA DPs (Fig. 12b–e). Moreover, upon increasing the PGlyMA DP, the surface roughness of vesicles was increased.

## Conclusion

In summary, a series of vinyl-functionalized macro-RAFT agents were synthesized by either the two-step RAFT polymerization of GMA and AMA or the one-step RAFT copolymerization of GMA and AMA. These macro-RAFT agents were then employed in aqueous photoinitiated RAFT dispersion polymerization of HPMA and cross-linked block copolymer nanoparticles with various morphologies were obtained. When using the block-type macro-RAFT agent, the presence of vinyl groups has little influence on the morphology of block copolymer nanoparticles. In contrast, using the random-type macro-RAFT agent could significantly promote the formation of higher-order morphologies. The effects of various reaction parameters on the morphology of block copolymer nanoparticles were investigated. It was found that a higher [HPMA]/[macro-RAFT] ratio, a shorter length of the stabilizer block, and a higher HPMA concentration facilitated the formation of higher-order morphologies. Finally, cross-linked worms and vesicles prepared by the aqueous photoinitiated RAFT dispersion polymerization using vinyl-functionalized macro-RAFT agents could be used as seeds for seeded RAFT polymerization of *t*BA or GlyMA. Nanoscale phase separation occurred within cross-linked block copolymer nanoparticles that enables further morphological control.

## Data availability

The data supporting this article have been included as part of the ESI.†

## Conflicts of interest

There are no conflicts to declare.

## Acknowledgements

## References

1 N. J. Warren and S. P. Armes, *J. Am. Chem. Soc.*, 2014, **136**, 10174–10185.
2 S. L. Canning, G. N. Smith and S. P. Armes, *Macromolecules*, 2016, **49**, 1985–2001.
3 N. J. W. Penfold, J. Yeow, C. Boyer and S. P. Armes, *ACS Macro Lett.*, 2019, **8**, 1029–1054.
4 W.-J. Zhang, C.-Y. Hong and C.-Y. Pan, *Macromol. Rapid Commun.*, 2019, **40**, 1800279.
5 X. Wang, L. Shen and Z. An, *Prog. Polym. Sci.*, 2018, **83**, 1–27.
6 F. Lv, Z. An and P. Wu, *CCS Chem.*, 2020, **3**, 2211–2222.
7 Z. Wu, W. Fang, C. Wu, N. Corrigan, T. Zhang, S. Xu and C. Boyer, *Chem. Sci.*, 2022, **13**, 11519–11532.
8 J. Yeow and C. Boyer, *Adv. Sci.*, 2017, **4**, 1700137.
9 J. Yeow, J. Xu and C. Boyer, *ACS Macro Lett.*, 2015, **4**, 984–990.
10 Y. Ding, M. Cai, Z. Cui, L. Huang, L. Wang, X. Lu and Y. Cai, *Angew. Chem., Int. Ed.*, 2018, **57**, 1053–1056.
11 L. Cao, Q. Zhao, Q. Liu, L. Ma, C. Li, X. Wang and Y. Cai, *Macromolecules*, 2020, **53**, 2220–2227.
12 J. I. Bowman, C. B. Eades, M. A. Vratsanos, N. C. Gianneschi and B. S. Sumerlin, *Angew. Chem., Int. Ed.*, 2023, **62**, e202309951.
13 G. M. Scheutz, J. I. Bowman, S. Mondal, J. Y. Rho, J. B. Garrison, J. Korpanty, N. C. Gianneschi and B. S. Sumerlin, *ACS Macro Lett.*, 2023, **12**, 454–461.
14 H. Sun, W. Cao, N. Zang, T. D. Clemons, G. M. Scheutz, Z. Hu, M. P. Thompson, Y. Liang, M. Vratsanos, X. Zhou, W. Choi, B. S. Sumerlin, S. I. Stupp and N. C. Gianneschi, *Angew. Chem., Int. Ed.*, 2020, **59**, 19136–19142.
15 S. W. Thompson, T. R. Guimarães and P. B. Zetterlund, *Polym. Chem.*, 2022, **13**, 5048–5057.
16 S. Chen, P. Shi and W. Zhang, *Chin. J. Polym. Sci.*, 2017, **35**, 455–479.
17 S. Li, G. Han and W. Zhang, *Polym. Chem.*, 2020, **11**, 4681–4692.
18 N. An, X. Chen and J. Yuan, *Polym. Chem.*, 2021, **12**, 3220–3232.
19 J. Cao, Y. Li, Y. Tan, L. Zhang and J. Tan, *Polym. Chem.*, 2024, **15**, 106–117.
20 Z. Li, R. Wang, X. Luo, L. Zhang and J. Tan, *Polym. Chem.*, 2024, **15**, 1736–1747.

21 Y. Li, Y. Li, R. Yan, L. Zhang, H. Liu and J. Tan, *Macromolecules*, 2024, **57**, 5175–5188.

22 W. Lin, S. Jia, Y. Li, L. Zhang, H. Liu and J. Tan, *ACS Macro Lett.*, 2024, **13**, 1022–1030.

23 B. Niu, H. Huang, L. Zhang and J. Tan, *ACS Macro Lett.*, 2024, **13**, 577–585.

24 R. Wang, W. Zhu, L. Zhang, X. Sheng and J. Tan, *Chin. J. Chem.*, 2024, **42**, 1606–1614.

25 J. He, Y. Chen, L. Zhang and J. Tan, *Chin. Chem. Lett.*, 2023, **34**, 107344.

26 S. Zhao, L. Zhang and J. Tan, *Chin. J. Chem.*, 2023, **41**, 1517–1525.

27 D. Lin, L. Zhang and J. Tan, *Acta Polym. Sin.*, 2023, **54**, 761–777.

28 Y. Li and S. P. Armes, *Angew. Chem., Int. Ed.*, 2010, **49**, 4042–4046.

29 W.-M. Wan, C.-Y. Hong and C.-Y. Pan, *Chem. Commun.*, 2009, 5883–5885.

30 C. Gao, J. Wu, H. Zhou, Y. Qu, B. Li and W. Zhang, *Macromolecules*, 2016, **49**, 4490–4500.

31 C. Gao, S. Li, Q. Li, P. Shi, S. A. Shah and W. Zhang, *Polym. Chem.*, 2014, **5**, 6957–6966.

32 W. Zhou, Q. Qu, W. Yu and Z. An, *ACS Macro Lett.*, 2014, **3**, 1220–1224.

33 Q. Qu, G. Liu, X. Lv, B. Zhang and Z. An, *ACS Macro Lett.*, 2016, **5**, 316–320.

34 S. W. Thompson, T. R. Guimarães and P. B. Zetterlund, *Macromolecules*, 2023, **56**, 9711–9724.

35 F. Ishizuka, H. J. Kim, D. Turkovic, R. P. Kuchel, S. Chatani, H. Niino and P. B. Zetterlund, *Macromolecules*, 2023, **56**, 4172–4180.

36 F. H. Sobotta, M. T. Kuchenbrod, F. V. Gruschwitz, G. Festag, P. Bellstedt, S. Hoeppener and J. C. Brendel, *Angew. Chem., Int. Ed.*, 2021, **60**, 24716–24723.

37 F. D'Agosto, J. Rieger and M. Lansalot, *Angew. Chem., Int. Ed.*, 2020, **59**, 8368–8392.

38 C. Gao, H. Zhou, Y. Qu, W. Wang, H. Khan and W. Zhang, *Macromolecules*, 2016, **49**, 3789–3798.

39 S. Qu, K. Wang, H. Khan, W. Xiong and W. Zhang, *Polym. Chem.*, 2019, **10**, 1150–1157.

40 A. Blanazs, A. J. Ryan and S. P. Armes, *Macromolecules*, 2012, **45**, 5099–5107.

41 Y. Pei and A. B. Lowe, *Polym. Chem.*, 2014, **5**, 2342–2351.

42 L. D. Blackman, K. E. B. Doncom, M. I. Gibson and R. K. O'Reilly, *Polym. Chem.*, 2017, **8**, 2860–2871.

43 J. Tan, D. Liu, Y. Bai, C. Huang, X. Li, J. He, Q. Xu, X. Zhang and L. Zhang, *Polym. Chem.*, 2017, **8**, 1315–1327.

44 Q. Zhang, R. Zeng, Y. Zhang, Y. Chen, L. Zhang and J. Tan, *Macromolecules*, 2020, **53**, 8982–8991.

45 X. Luo, S. Zhao, Y. Chen, L. Zhang and J. Tan, *Macromolecules*, 2021, **54**, 2948–2959.

46 E. R. Jones, M. Semsarilar, P. Wyman, M. Boerakker and S. P. Armes, *Polym. Chem.*, 2016, **7**, 851–859.

47 Y. Zhang, M. Cao, G. Han, T. Guo, T. Ying and W. Zhang, *Macromolecules*, 2018, **51**, 5440–5449.

48 D. Ikkene, A. A. Arteni, M. Ouldali, G. Francius, A. Brûlet, J.-L. Six and K. Ferji, *Biomacromolecules*, 2021, **22**, 3128–3137.

49 D. Ikkene, A. A. Arteni, H. Song, H. Laroui, J.-L. Six and K. Ferji, *Carbohydr. Polym.*, 2020, **234**, 115943.

50 P. G. Georgiou, I. Kontopoulou, T. R. Congdon and M. I. Gibson, *Mater. Horiz.*, 2020, **7**, 1883–1887.

51 X. Wang, C. A. Figg, X. Lv, Y. Yang, B. S. Sumerlin and Z. An, *ACS Macro Lett.*, 2017, **6**, 337–342.

52 W. Cai, S. Yang, L. Zhang, Y. Chen, L. Zhang and J. Tan, *Macromolecules*, 2022, **55**, 5775–5787.

53 S. Yang, L. Zhang, Y. Chen and J. Tan, *Macromolecules*, 2022, **55**, 8472–8484.

54 W. Hou, Z. Li, L. Xu, Y. Li, Y. Shi and Y. Chen, *ACS Macro Lett.*, 2021, **10**, 1260–1265.

55 W. Hou, J. Wu, Z. Li, Z. Zhang, Y. Shi and Y. Chen, *Macromolecules*, 2023, **56**, 824–832.

56 J. Xu and C. Boyer, *Macromolecules*, 2015, **48**, 520–529.

57 A. Blanazs, J. Madsen, G. Battaglia, A. J. Ryan and S. P. Armes, *J. Am. Chem. Soc.*, 2011, **133**, 16581–16587.

58 J. He, D. Liu, J. Tan and L. Zhang, *Polymer*, 2018, **145**, 70–79.

59 J. Kadirkhanov, C.-L. Yang, Z.-X. Chang, R.-M. Zhu, C.-Y. Pan, Y.-Z. You, W.-J. Zhang and C.-Y. Hong, *Polym. Chem.*, 2021, **12**, 1768–1775.

60 L. Zhang, Q. Lu, X. Lv, L. Shen, B. Zhang and Z. An, *Macromolecules*, 2017, **50**, 2165–2174.

61 M. Chen, J.-W. Li, W.-J. Zhang, C.-Y. Hong and C.-Y. Pan, *Macromolecules*, 2019, **52**, 1140–1149.

62 S. Sugihara, S. P. Armes, A. Blanazs and A. L. Lewis, *Soft Matter*, 2011, **7**, 10787–10793.

63 S. J. Byard, M. Williams, B. E. McKenzie, A. Blanazs and S. P. Armes, *Macromolecules*, 2017, **50**, 1482–1493.

64 B. Zhang, X. Lv, A. Zhu, J. Zheng, Y. Yang and Z. An, *Macromolecules*, 2018, **51**, 2776–2784.

65 X. Dai, Y. Zhang, L. Yu, X. Li, L. Zhang and J. Tan, *ACS Macro Lett.*, 2019, **8**, 955–961.

66 J. He, J. Cao, Y. Chen, L. Zhang and J. Tan, *ACS Macro Lett.*, 2020, **9**, 533–539.

67 G. Li, N. Xu, Q. Yu, X. Lu, H. Chen and Y. Cai, *Macromol. Rapid Commun.*, 2014, **35**, 1430–1435.

68 J. Zhou, Q. Huang, L. Zhang and J. Tan, *ACS Macro Lett.*, 2023, **12**, 1457–1465.

69 J. Ma, C. Cheng, G. Sun and K. L. Wooley, *Macromolecules*, 2008, **41**, 9080–9089.

70 G. Xie, J. Wu, L. Zhang and J. Tan, *Langmuir*, 2024, **40**, 17098–17108.

71 J. Tan, X. Dai, Y. Zhang, L. Yu, H. Sun and L. Zhang, *ACS Macro Lett.*, 2019, **8**, 205–212.

72 P. Chambon, A. Blanazs, G. Battaglia and S. P. Armes, *Macromolecules*, 2012, **45**, 5081–5090.

73 J. Wu, L. Zhang, Y. Chen and J. Tan, *ACS Macro Lett.*, 2022, **11**, 910–918.